AIP | Journal of Applied Physics

Modification of ultrananocrystalline diamond film microstructure via Fe-coating and annealing for enhancement of electron field emission properties

Kuang-Yau Teng, Wen-Ching Shih, Pin-Chang Huang, Huang-Chin Chen, Chen-Yau Tang, and I-Nan Lin

Citation: Journal of Applied Physics **112**, 033708 (2012); doi: 10.1063/1.4739772
View online: http://dx.doi.org/10.1063/1.4739772
View Table of Contents: http://scitation.aip.org/content/aip/journal/jap/112/3?ver=pdfcov
Published by the AIP Publishing

Modification of ultrananocrystalline diamond film microstructure via Fe-coating and annealing for enhancement of electron field emission properties

Kuang-Yau Teng,[1] Wen-Ching Shih,[2] Pin-Chang Huang,[2] Huang-Chin Chen,[1] Chen-Yau Tang,[1] and I-Nan Lin[1,a)]
[1]*Department of Physics, Tamkang University, Tamsui, New-Taipei 251, Taiwan*
[2]*Graduate Institute in Electro-Optical Engineering, Tatung University, Taipei 104, Taiwan*

(Received 9 January 2012; accepted 2 July 2012; published online 3 August 2012)

The interaction between Fe-coatings and ultrananocrystalline diamond (UNCD) films during annealing was investigated in detail using transmission electron microscopy. The thin Fe-coating first formed nanosized Fe-clusters and then catalytically dissociated the diamond, re-precipitating carbon to form nanosized graphite clusters. These clusters formed conducting networks that facilitated electron transport and greatly improved the electron field emission (EFE) properties of the UNCD films. The extent of enhancement varied markedly with annealing temperature and atmosphere. For H_2-annealed films, EFE behavior was optimized by annealing at 900 °C. EFE was turned on at $(E_0)_{H2} = 1.2\ V/\mu m$, attaining EFE current density of $(J_e)_{H2} = 772.0\ \mu A/cm^2$ at an applied field of 8.8 V/mm. These characteristics were superior to those of UNCD films NH_3-annealed at 850 °C. The inferior EFE properties for the NH_3-annealed samples were attributed to reaction of NH_3 with the hydrocarbon phase that encapsulated the nanosized diamond grains, hindering Fe–diamond interaction. © *2012 American Institute of Physics*. [http://dx.doi.org/10.1063/1.4739772]

I. INTRODUCTION

Diamond films possess many desirable physical and chemical properties[1–3] and have been the focus of intensive research, since their successful synthesis in a low pressure and low temperature chemical vapor deposition (CVD) process.[4] Due to the negative electron affinity (NEA)[5] characteristics of their re-constructed (100) surface, diamond films are considered to have great potential as electron field emitters.[6,7] However, the large electronic band gap (5.1 eV) of diamond films hinders their electron field emission (EFE) behavior tremendously due to a lack of conducting electrons required for field emission. Doping diamond films with boron or nitrogen species introduces abundant interband energy levels, which enhances the supply of electrons and markedly improve the EFE properties of the materials.[8–11] However, these properties are still not satisfactory because most of the emitting surfaces of diamond are not re-constructed (100) surfaces and thus do not possess NEA characteristics. Modification of the diamond surface to enhance EFE has thus been a main focus of research.[12–16] Among various approaches, thin metallic coatings have been reported to significantly influence the EFE properties of diamond films,[13,14] but the related mechanism is not clear. Recently, Huang *et al*. investigated the evolution of microstructure in Fe-coated/annealed microcrystalline diamond (MCD) films[15,16] and attributed the enhancement in their EFE properties to the formation of nanographite by Fe–diamond interaction. However, this interaction only occurred at the surface of the MCD films. Transport of electrons from the substrate through the MCD films to their surface was not improved because they contained large grains with grain boundaries of insignificant thickness that did not give efficient electron transport. Thus, the EFE behavior of the MCD films was not fully developed. In contrast, ultrananocrystalline diamond (UNCD) films have been found to contain ultra-small grains with grain boundaries of considerable thickness, which were presumed to contain sp^2-carbon phase and efficiently conducted electrons.[17,18] Thus, the conductivity of electrons from substrate to surface in UNCD films has been found to be markedly better than that in MCD films. It is expected that enhancing the surface conductivity of such UNCD films via Fe-coating/annealing processes will further enhance their EFE properties.

In this paper, the effect of Fe-coating and annealing processes on surface characteristics and EFE behavior of UNCD films was examined systematically. Transmission electron microscopy (TEM) was used to investigate the microstructure of the films and the possible mechanism was discussed based on the observations.

II. EXPERIMENTAL

Ultrananocrystalline diamond films were grown on p-type silicon substrate by a microwave plasma enhanced CVD (MPE-CVD) process. The Si wafer substrates were first thoroughly cleaned by sequential rinsing in dilute aqueous solutions of hydrogen peroxide/ammonium hydroxide and hydrogen peroxide/hydrochloric acid. The cleaned Si-substrates were then ultrasonicated in methanol containing nanosized (<32.5 nm) diamond and Ti powders for 45 min. The substrates were ultrasonicated again in methanol to remove any nanoparticles adhered to the Si-substrates. The UNCD films were grown for 1 h in $CH_4(2\%)/H_2(6\%)/Ar$ plasma excited by a 1200 W (2.45 GHz) microwave, at a

a)Author to whom correspondence should be addressed. Electronic mail: inanlin@mail.tku.edu.tw.

pressure of 150 Torr and total flow rate of 200 sccm. The resulting films were then coated with a thin layer of Fe (~5 nm) by DC sputtering and thermally annealed at 800–950 °C in an NH_3 (or H_2) atmosphere for 5 min, with heating and cooling rates of 15 °C/min and gas flow rate of 100 sccm.

The morphology and structure of the films were investigated using scanning electron microscopy (SEM, Joel JSM-6500F) and Raman spectroscopy (Renishaw), respectively. A UV laser (325 nm) with a low power of 5 mV was used for Raman measurements. The detailed microstructure of the films was examined using TEM (Joel 2100). EFE properties of the diamond films were measured using a parallel plate setup, in which indium-tin oxide coated glass plate was used as the anode. The cathode-to-anode distance was set with a fixed spacer (125 μm) and the emission area was controlled using a circular opening in the spacer of about 8 mm in diameter. Current–voltage (I–V) characteristics of the films were acquired using a Keithley 2410 at 10^{-6} Torr and were normalized with respect to the area of the emission and the cathode-to-anode distance to give current density-applied field (J-E) curves. EFE properties were analyzed using the Fowler-Nordheim (F-N) model,[19] and the turn-on field was designated as the interception of the straight lines extrapolated from the high-field and low-field segments of the F-N plots.

III. RESULTS

Figure 1(a) shows the SEM morphology of the as-grown UNCD films, indicating that the films had a nanograin microstructure with a uniform size distribution of diamond grains. However, TEM examination showed that the UNCD films actually contained a duplex microstructure (Fig. 1(b)), with large diamond aggregates (~100 nm in size) distributed evenly among a matrix of ultra-small equiaxed grains (~5 nm in size). The spotty diffraction rings observed in the selected area electron diffraction (SAED) patterns shown in the inset of Fig. 1(b) confirmed the presence of large diamond aggregates. The ring arrangement of the spots implied that the diamond grains were randomly oriented.

Figure 1(c) shows that the as-grown UNCD films gave very unique Raman spectra. In addition to a sharp Raman resonance peak at 1332 cm^{-1} (D-band), there were many diffused peaks, including υ_1-band (1140 cm^{-1}), υ_3-band (1480 cm^{-1}), D*-band (1350 cm^{-1}), and G-band (1580 cm^{-1}). The sharp D-band resonance peak represents the diamond lattice Γ_{2g} band, usually observed for diamond with grains larger than hundreds of nanometers. The diffused resonance peaks (υ_1-, υ_3-, D*-, and G-bands) are usually observed for diamond with ultra-small grain microstructure. The υ_1- and υ_3-bands represent trans-polyacetylene (t-PA) present along grain boundaries,[20,21] whereas the D*- and G-bands represent disordered carbon and graphitic phase[22,23] contained in the diamond grains. The simultaneous occurrence of sharp and diffused resonance peaks indicated coexistence of large and ultra-small diamond grains, in accordance with TEM observations. Figure 1(d) shows that EFE in the as-grown UNCD films was turned on at

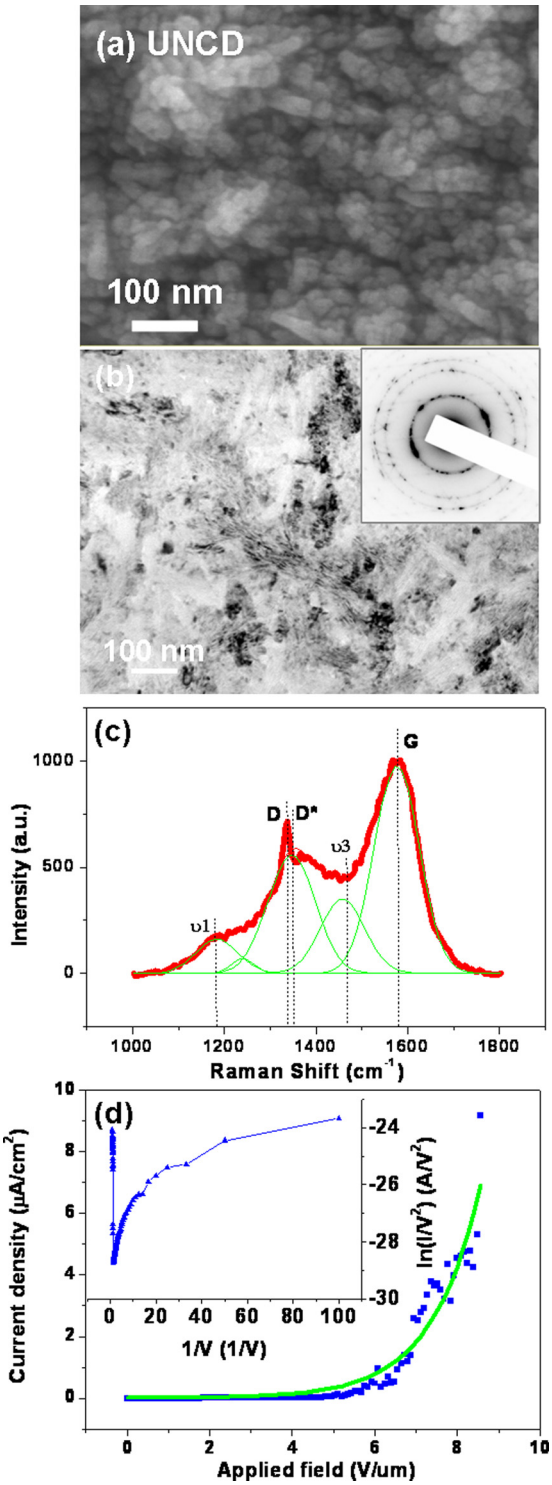

FIG. 1. (a) SEM micrograph, (b) TEM micrograph with SAED inset, (c) Raman spectrum, and (d) EFE properties with inset showing the Fowler-Nordheim plot of the J-E curve of the as-prepared UNCD films. The UNCD films were grown in CH_4(2%)/H_2(6%)/Ar plasma.

$E_0 = 3.9$ V/μm, achieving $J_e = 8.9$ μA/cm^2 at an applied field of 8.8 V/μm.

Coating with a thin layer of Fe (~5 nm) almost completely suppressed the EFE properties of the films (not shown), but the annealing process that followed restored EFE behavior. The resulting EFE performance was even better than that of the pristine UNCD films, with the extent of

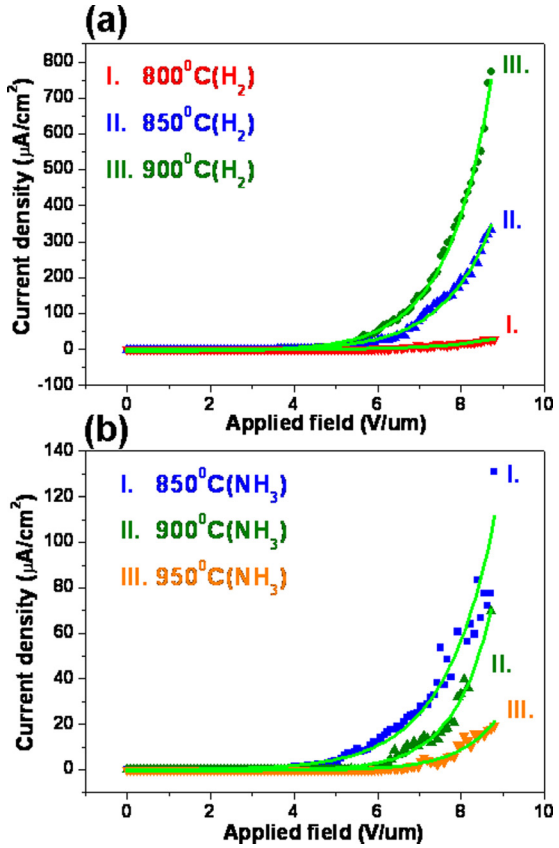

FIG. 2. EFE properties of UCND films grown in $CH_4/H_2/Ar$ plasma ($H_2 = 6\%$) and Fe-coated/annealed in (a) H_2 atmosphere at 800–900 °C and (b) NH_3 atmosphere at 850-950 °C.

enhancement varying with annealing temperature. Figure 2(a) shows that for Fe-coated and H_2-annealed UNCD films, the turn-on field (E_0) decreased and the EFE current density (J_e) increased with increasing annealing temperature. The best EFE properties were observed for UNCD films H_2-annealed at 900 °C. The EFE process was turned on at 1.2 V/μm, attaining EFE current density of 771.0 μA/cm^2 at an applied field of 8.8 V/μm (curve III, Fig. 2(a)). Important EFE parameters, including turn-on field (E_0) and EFE current density (J_e), at an applied field of 8.8 V/μm were extracted from the J-E curves and are listed in Table I(a). The Raman characteristics of the films were not markedly altered by the H_2-annealing process (Fig. 3(a)). The only exceptions were that H_2-annealing at 900 °C induced a large broadening of the Raman resonance peak (at 1405 cm^{-1}) and a slight blue-shift of the G-band resonance peak to around 1600 cm^{-1} (curve III, Fig. 3(a)), implying the presence of crystalline graphite phase. The significance of this phenomenon will be discussed shortly. SEM morphology was not markedly altered by post-annealing in H_2 atmosphere (not shown).

TABLE I. EFE performance of UCND films after Fe-coating/annealing in (a) H_2 or (b) NH_3 atmosphere, and (c) as-deposited. The films were grown in $CH_4/H_2/Ar = 4/12/184$ sccm plasma excited by 1200 W microwave (at 150 Torr).

Samples	Annealing atmosphere	Annealing temperature (°C)	E_0[a] (V/μm)	J_e[b] (μA/cm^2)
$UNCD_{an(H2)}$	H_2	800 °C	2.6	28
		850 °C	2.4	335
		900 °C	1.2	771
$UNCD_{an(NH_3)}$	NH_3	850 °C	1.0	166
		900 °C	2.8	70
		950 °C	4.7	19
UNCD	—	—	3.9	8.9

[a]E_0: turn-on field designated as the interception of the lines extrapolated from the high field and low field segments in F-N plot.
[b]J_e: field emission current density measured at 8.8 V/μm.

Previous studies[15,16] on Fe-coating/annealing of MCD films reported that the Fe-coating formed clusters prior to the annealing step. The annealing process catalytically dissociated the sp^3-bonded diamond lattices and then re-precipitated carbon on the opposite side of the Fe-clusters to form few-layer graphite. To understand whether similar Fe–diamond interaction also occurred in the present UNCD films, the Fe-coated/annealed samples were investigated using TEM. It should be noted that only UNCD samples that exhibited the best EFE properties (i.e., H_2-annealed at 900 °C) were examined. Figure 4(a) shows that the H_2(900 °C)-annealed UNCD films retained the duplex granular structure, i.e., large diamond aggregates distributed among a matrix of ultra-small diamond grains. Detailed analyses of the SAED (inset Fig. 4(a)) showed that in addition to the diamond diffraction rings, there existed an extra faint diffraction ring of smaller diameter than the diamond (111) ring. This extra diffraction ring corresponded to Fe_3C phase, which will be further analyzed shortly.

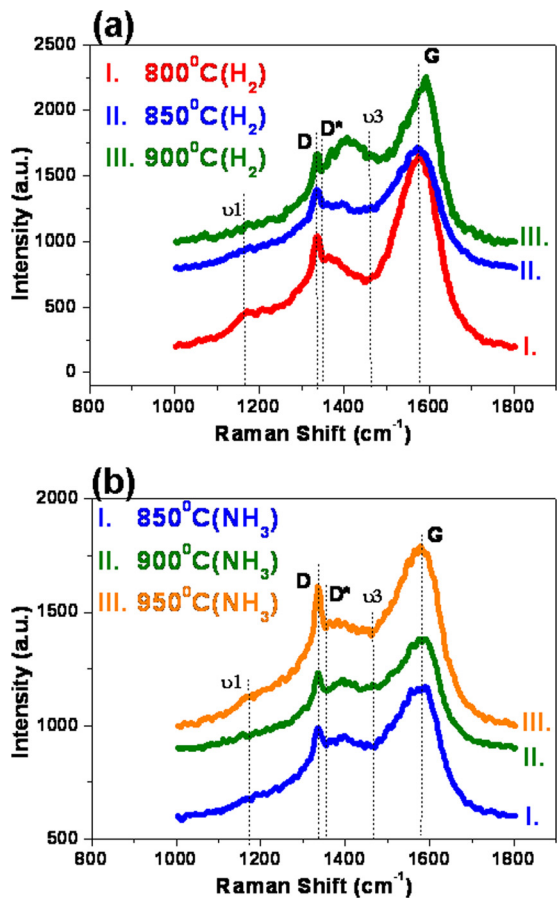

FIG. 3. Raman spectra of UCND films grown in $CH_4/H_2/Ar$ plasma ($H_2 = 6\%$) and Fe-coated/annealed in (a) H_2 atmosphere at 800–900 °C and (b) NH_3 atmosphere at 850–950 °C.

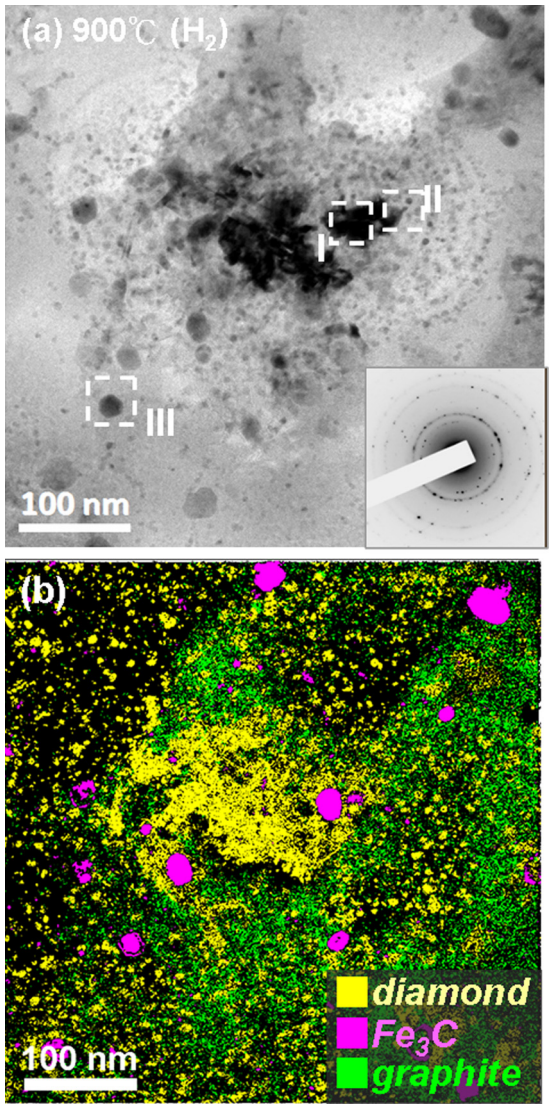

FIG. 4. (a) TEM bright field image (BF) with SAED inset and (b) composed dark field image (c-DF), the superposition of dark field images taken using diffraction spots corresponding to diamond, Fe_3C, and graphite, for Fe-coated UNCD films H_2-annealed at 900 °C for 5 min.

Figure 5(a) shows that the large aggregates, corresponding to region I in Fig. 4(a), contained a large proportion of stacking fault (area 1) and hexagonal diamond (area 2) defects. The presence of stacking faults was indicated by rel-rods observed along the major diffraction spots in the Fourier-transformed diffractogram (FT_{0a}) corresponding to the whole structure image, whereas the existence of hexagonal diamond was implied by the systematic row of diffraction spots in FT_{0a}. Such faults are common planar defects in diamond aggregates, and are induced by CH_4/Ar plasma containing a few percent H_2.[24] Figure 5(b) shows the detailed microstructure of region II in Fig. 4(a), adjacent to the diamond aggregates. The FT image (FT_{0b}) corresponding to the structural image in Fig. 5(b) indicated the presence of Fe_3C phase (designated as "Fe_3C" in FT_{ob}) and graphitic phase (designated as "*g*"), in addition to the diamond (designated as "*d*"). Detailed analysis revealed that the large clusters in this region (area 3) were Fe_3C particulates, as illustrated by the FT image FT_3. Moreover, curved fringes (indicated by the arrow in Fig. 5(b)) appeared on the other side of the Fe_3C particulates against the diamond. FT image FT_4 indicates that these curved fringes were nanosized graphite phase. The Fe_3C particulates were around 10–20 nm in size and the graphite layer was around 2–3 nm in thickness. Thus, Figure 5(b) clearly infers that the graphite phase was induced by the interaction of nanosized Fe-clusters with the diamond. Presumably, the Fe-clusters catalytically dissociated the diamond and re-precipitated the carbon to form few-layer graphite. These Fe-clusters were formed by coalescence of the Fe-coating prior to the onset of Fe–diamond interaction while ramping up to the annealing temperature, whereas the Fe_3C particulates were created during cooling when carbon dissolved in the Fe-clusters was frozen inside them.

Moreover, Fig. 4(a) shows the existence of abundant spherical particulates, around 20 nm in size, similar the ones found in region III. Figure 5(c) shows the enlarged TEM micrograph of these particulates. The FT image (FT_{0c}) shown inset in Fig. 5(c) reveals that this region contained Fe_3C and graphite phases in addition to the diamond. FT image (FT_5) clearly illustrates that the particulate (area 5) was a Fe_3C cluster. Nanosized graphite clusters appeared near the periphery of the Fe_3C particulates, such as that in area 6 (FT_6). There were also nanographite clusters located in the middle of Fe_3C clusters, such as in area 7 (FT_7). Presumably, these nanographite clusters were above or beneath the Fe_3C clusters, rather than inside them. These results imply, again, that the nanographite particulates were induced by interaction of Fe-clusters with diamond.

The constituent phases of the present UNCD films were best illustrated by composed dark field image (c-DF), which is the superposition of dark field images acquired using diffraction spots corresponding to diamond, Fe_3C, and graphite phases. Figure 4(b) shows the c-DF image corresponding to the bright field image in Fig. 4(a), indicating that the UNCD films Fe-coated/annealed in H_2 (900 °C) contained, in addition to the diamond grains (yellow color), abundant Fe_3C particulates (pink color) and graphite phase (green color). Restated, the nanographite clusters were actually induced almost everywhere in the Fe-coated/H_2-annealed UNCD films. It should be noted that Fe_3C particle also possesses metallic conductivity.[25] Apparently, the induction of graphite and Fe_3C phase is the prime factor improving the EFE properties of the UNCD films when they are Fe-coated/H_2-annealed in at 900 °C.

To enhance EFE properties of UNCD films, it is critical to control the parameters of the Fe-coating/annealing processes. Fe-coatings of other thicknesses or annealing at other temperatures all led to inferior EFE properties (not shown) compared with those illustrated in Fig. 2(a) and Table I. Only the EFE properties of the samples showing improved characteristics were discussed. Interestingly, annealing of UNCD films in other kinds of reducing atmosphere, such as NH_3, also resulted in significantly different EFE property behavior. Figure 2(b) and Table I indicate that, after annealing in NH_3 atmosphere, EFE properties changed with annealing temperature in an opposite trend to those heat-treated in H_2 atmosphere. For these samples, E_0 increased and J_e decreased with increase in post-annealing temperature. The best EFE

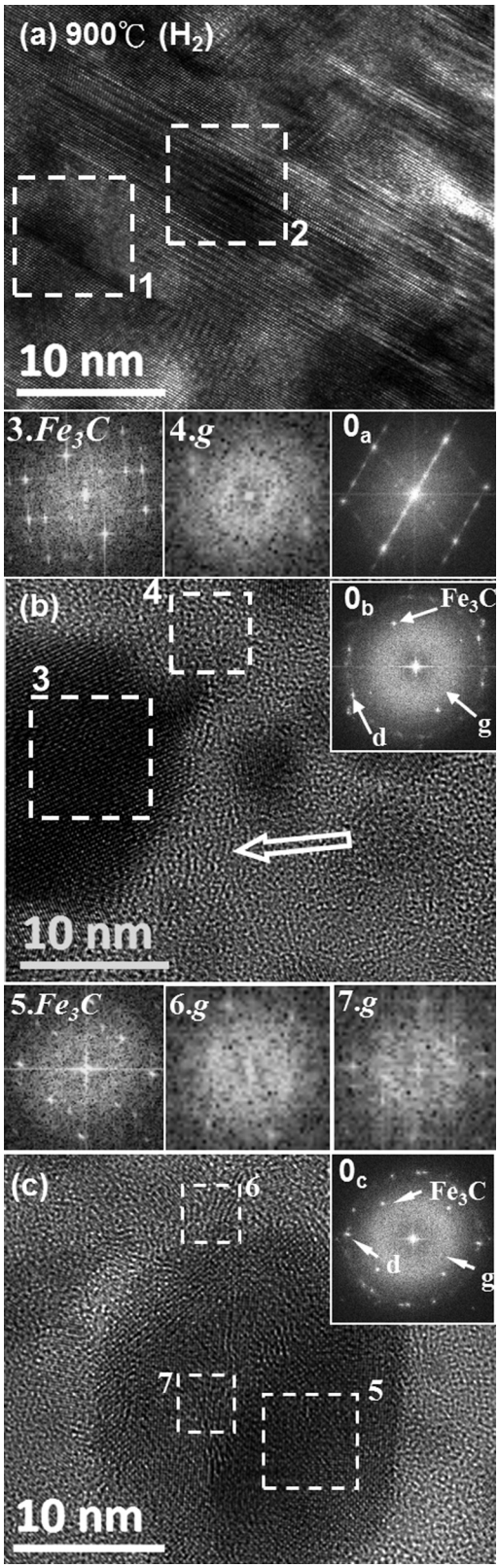

FIG. 5. TEM images corresponding to (a) region I, (b) region II, and (c) region III in Fig. 4(a) for Fe-coated UNCD film H_2-annealed at 900 °C for 5 min. Fourier-transformed diffractograms corresponding to the designated areas are shown inset.

properties obtainable for UNCD films NH_3-annealed at 850 °C were $(E_0)_{an} = 1.0\,V/\mu m$ and $(J_e)_{an} = 166.0\,\mu A/cm^2$ at an applied field of $8.8\,V/\mu m$. Annealing at lower temperature did not restore the EFE properties of the films. Moreover, while the emission current (J) of the H_2-annealed films increased smoothly with the applied field (E), those of NH_3-annealed films fluctuated slightly (cf. Figs. 2(a) and 2(b)). This result indicated that H_2-annealing was more efficient in improving the EFE properties of the UNCD films than NH_3-annealing.

Figure 3(b) shows that the Raman characteristics of the UNCD films essentially did not change after Fe-coating and NH_3-annealing in the chosen temperature range. SEM morphology also did not change (not shown). Detailed investigation of the evolution of microstructure during Fe-coating/NH_3-annealing by TEM was also performed to understand the related mechanism. Figure 6(a) shows that the UNCD films Fe-coated/NH_3-annealed at 850 °C also contained a duplex granular structure, i.e., large diamond aggregates (around 50–200 nm in size) sparsely distributed among a matrix of ultra-small grains. The inset in Fig. 6(a) shows spotty diffraction rings in the SAED, attributed to the presence of large aggregates in the films. Notably, the SAED of this

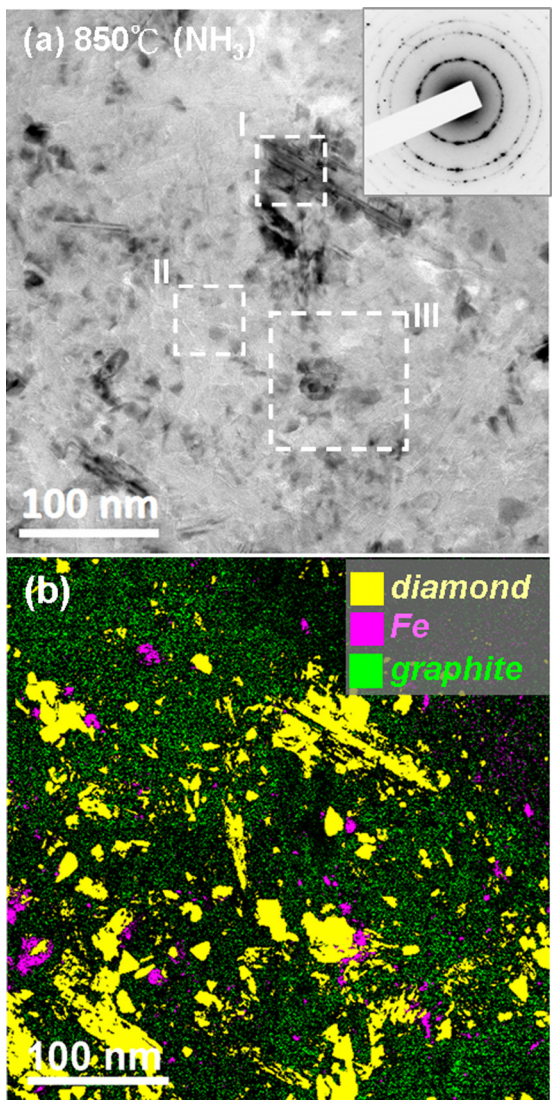

FIG. 6. (a) TEM bright field image (BF) with SAED inset and (b) composted dark field image, (c-DF), the superposition of dark field images taken using diffraction spots corresponding to diamond, Fe, and graphite for Fe-coated UNCD film NH_3-annealed at 850 °C for 5 min.

sample contained only diamond diffraction rings and no extra diffraction ring corresponding to Fe_3C was observable. The significance of such an observation will be discussed shortly.

Figure 7(a), a TEM image of large diamond aggregate (region I, Fig. 6(a)), reveals that the diamond aggregates were also heavily faulted. The FT_{0a} corresponding to the whole structure image shown in Fig. 7(a) indicated, again, that this region contained stacking faults (area 1, FT_1) and hexagonal diamond (area 2, FT_2). A TEM image corresponding to a small cluster region (region II, Fig. 6(a)) is shown in Fig. 7(b). The FT image (FT_{0b}) corresponding to the whole structure image shown in Fig. 7(b) exhibited a strong diffused ring in the center of image in addition to the spotty diffraction ring. The central diffuse ring indicated the existence of a large proportion of graphitic (or amorphous carbon) phase in these samples, whereas the diffraction spots corresponded to randomly oriented diamond grains. A typical example of nanographite clusters is shown in area 3 (and FT_3), while that of nanodiamond is highlighted in area 4 (and FT_4). The proportion of graphitic phase was markedly smaller compared with that in the H_2-annealed samples (cf. Fig. 5(b)). Notably, there was no Fe_3C phase observable in these samples.

The Fe–diamond interaction zone for the 850 °C (NH_3) annealed diamond films is better demonstrated in the TEM micrographs presented in Fig. 8, which correspond to region III in Fig. 6(a). It should be noted that the samples corresponding to Fig. 8(a) were tilted slightly so that the diamond aggregates were out of contrast and the non-diamond phase

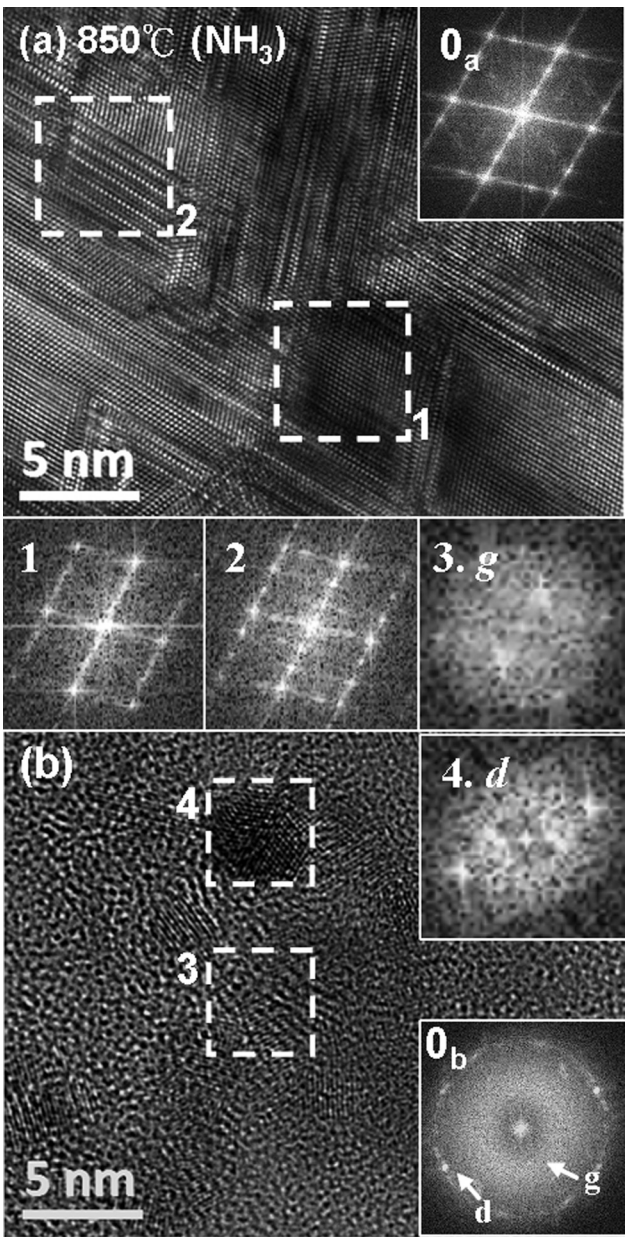

FIG. 7. Structural TEM image of (a) large diamond aggregates (region I in Fig. 6(a)) and (b) ultra-small grain region (region II in Fig. 6(a)) of Fe-coated UNCD film NH_3-annealed at 850 °C for 5 min.

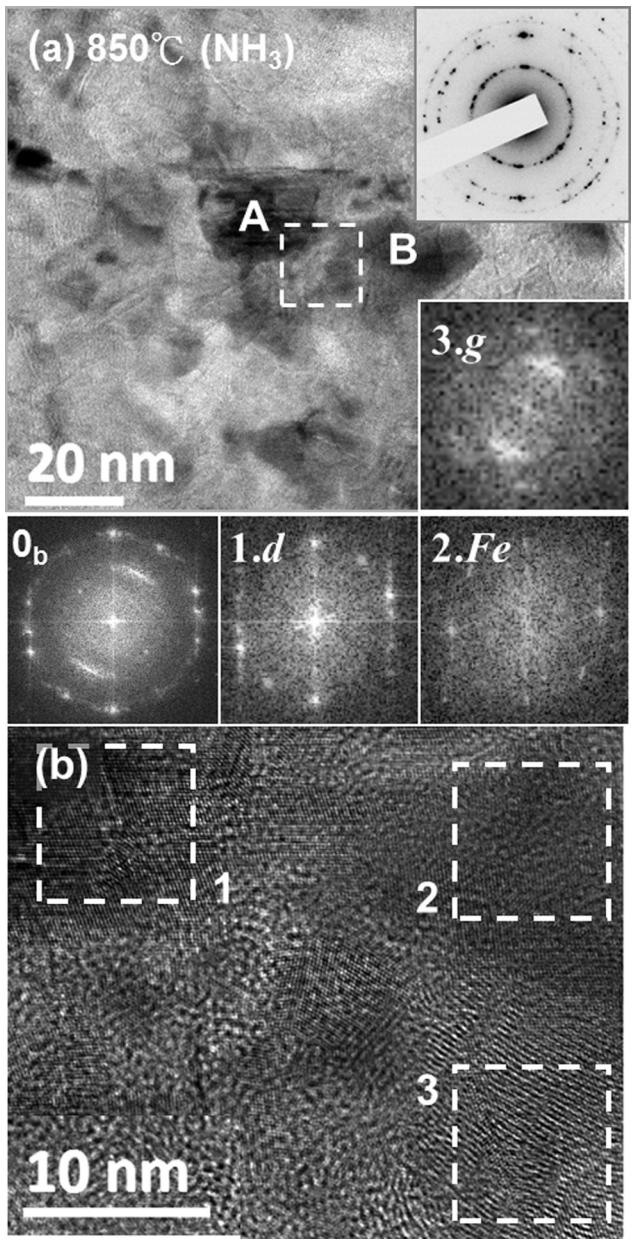

FIG. 8. (a) TEM bright field micrograph and (b) structural image of region III in Fig. 6(a) of Fe-coated UNCD film NH_3-annealed at 850 °C for 5 min, showing the presence of Fe-particulates near the diamond grains and nanographite clusters near the Fe-particulates. FT_{0b} is the Fourier-transformed diffractogram corresponding to the whole region in "b," and FT_1 to FT_3 are FT images corresponding to areas 1 to 3 in "b."

constituents in this region could be more clearly resolved. Figure 8(b) shows the TEM image of the region designated in Fig. 8(a). The FT image (FT_{0b}) corresponding to the whole structure image in Fig. 8(b) shows, again, that this region consisted of diamond, graphite, and Fe-related particulates. Detailed analysis of Fig. 8(b) indicated that area 1, corresponding to particulates A in Fig. 8(a), was a diamond grain (FT_1) and area 2, corresponding to particulates B in Fig. 8(a), was an Fe-cluster (FT_2). Area 3 (FT_3), the other side of the Fe-clusters against the diamond, contained a large proportion of nanographite. Such a microstructure, with coexistence of nanodiamond, Fe-clusters, and nanographite particulates, is similar to those observed in the literature for Fe-coated/annealed MCD films. It can be assumed, therefore, that similar Fe–diamond interaction to that observed in the H_2-annealed films also occurred when the UNCD films were Fe-coated and NH_3-annealed at 850 °C.

To more clearly illustrate the phase constituents of the Fe-coated/annealed UNCD films, a dark field image was again composed by superimposing dark field images taken using diffraction spots corresponding to diamond, Fe, and graphite. Figure 6(b) shows the composed DF image corresponding to the BF image in Fig. 6(a), revealing that besides the diamond grains, there were small clusters of Fe particulates sparsely but evenly distributed in the samples. In addition, the nanographite particulates were small in size, but were densely and uniformly distributed all over the UNCD films. Moreover, the Fe_3C phase was small in proportion that it could not be clearly observed in Fig. 6(b). The significance of such an observation will be discussed shortly.

Figure 2 and Table I show that, for the present UNCD films, the H_2-annealing process led to larger EFE current density and smoother J-E behavior than the NH_3-annealing process. While it is evident that Fe–diamond interaction can also account for the observed improvement in EFE properties of the UNCD films after Fe-coating and subsequent annealing in reducing atmosphere (NH_3 or H_2), it was still not clear why H_2-annealed UNCD films possessed markedly superior EFE properties to NH_3-annealed films. It should be reminded that the composed DF images (cf. Figs. 4(b) and 6(b)) revealed that most of the Fe-clusters were transformed into Fe_3C particulates, along with the presence of a large proportion of nanographite clusters, when the UNCD films were H_2-annealed (cf. Fig. 4(b)). In contrast, a large proportion of Fe-clusters remained untransformed and the proportion of nanographite clusters was smaller when the films were NH_3-annealed (cf. Fig. 6(b)). This phenomenon was more clearly illustrated by the linear diffraction patterns (*ldps*) in Fig. 9, where the *lpds* were deduced from the SAEDs of 900 °C (H_2) and 850 °C (NH_3) annealed samples shown as inset in Figs. 4(a) and 6(a), respectively. Fe_3C diffraction peaks were observable for the H_2-annealed film (curve I, Fig. 9), but only the Fe diffraction peak was observable for the NH_3-annealed film (curve II, Fig. 9). Thus, it seems that the interaction of Fe and diamond was somehow hindered during NH_3-annealing. Whether the absence of Fe_3C phase is the factor causing the inferior EFE properties of the NH_3-annealed films is not clear in this moment. More systematic investigation is needed to clarify such a phenomenon.

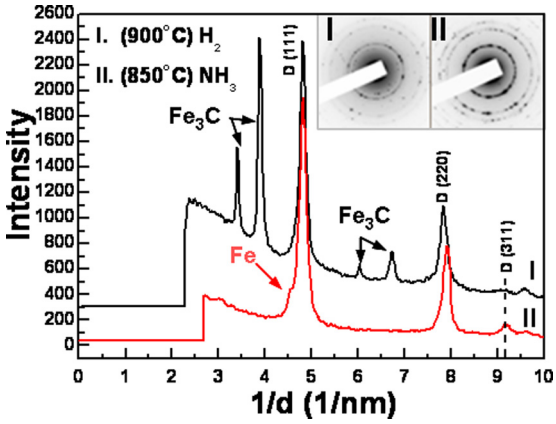

FIG. 9. Linear diffraction patterns (*ldp*) for Fe-coated UNCD films annealed in (I) H_2 (900 °C) and (II) NH_3 (850 °C) for 5 min. *ldp* patterns were deduced from SAED, shown as insets in Figs. 4(a) and 6(a), respectively.

It is known that UNCD films consist of ultra-small grains with grain boundaries of considerable thickness.[26,27] These nanosized diamond grains are encapsulated by a thin layer of hydrocarbon, presumably t-PA.[24] When the present samples were annealed in H_2-atmosphere, atomic hydrogen was able to efficiently etch out the hydrocarbon layer encapsulating the nanosized diamond grains, which triggered interaction between Fe-clusters and diamond. In contrast, when the samples were annealed in NH_3-atmosphere, atomic nitrogen may have interacted with the hydrocarbon layer, forming a more stable hydro-nitro-carbon layer that hindered the interaction of Fe-clusters and diamond. Therefore, NH_3-annealing showed less efficiency in improving the EFE properties of UNCD films compared with H_2-annealing.

IV. CONCLUSIONS

Modification of UNCD film microstructure via Fe-coating and annealing processes was investigated in detail using TEM. The Fe-coating was found to form small Fe-clusters prior to the onset of Fe-to-diamond interaction. At the annealing temperature, the Fe-clusters catalytically dissolved carbon in the diamond grains and re-precipitated them to form nanosized graphite clusters. The nanographite clusters not only existed near the large diamond aggregates but were also present among the ultra-small diamond grains. The nanographite phase formed an interconnected path for electron transport, and the EFE properties of the UNCD films were thus greatly improved. However, the observed enhancement in EFE properties of the UNCD films not only varied with annealing temperature but also changed with annealing atmosphere. EFE was found to turn on at $(E_0)_{H2} = 1.2\,V/\mu m$, attaining EFE current density of $(J_e)_{H2} = 771\,\mu A/cm^2$ at an applied field of $8.8\,V/\mu m$, in the Fe-coated UNCD films H_2-annealed at 900 °C. In contrast, for those which were NH_3-annealed at 850 °C, EFE was initiated at $(E_0)_{NH3} = 1.0\,V/\mu m$, attaining smaller EFE current density of $(J_e)_{NH3} = 166\,\mu A/cm^2$ under the same applied field. These inferior EFE properties were attributed to interaction of NH_3 with the hydrocarbon layer encapsulating the nanosized diamond grains, hindering Fe–diamond interaction.

ACKNOWLEDGMENTS

Financial support from the National Science Council, R. O. C. through project NSC99-2119 -M-032-003-MY2 is gratefully acknowledged. W. C. Shih and P. C. Huang would also like to thank Tatung University for financial support.

[1]J. E. Field, *The Properties of Diamonds* (Academic, London, 1979).
[2]H. Liu and D. S. Dandy, Diamond Relat. Mater. **4**, 1173 (1995).
[3]J. C. Angus, H. A. Will, and W. S. Stanko, J. Appl. Phys. **39**, 2915 (1968).
[4]B. V. Spitsyn, L. L. Bouilov, and B. V. Derjaguin, J. Cryst. Growth **52**, 219 (1981).
[5]J. van der Weide, Z. Zhang, P. K. Baumann, M. G. Wensell, J. Bernholc, and R. J. Nemanich, Phys. Rev. B **50**, 5803 (1994).
[6]M. W. Geis, N. N. Efremow, J. D. Woodhouse, M. D. Mcaleese, M. Marchywka, D. G. Socker, and J. F. Hochedez, IEEE Electron Device Lett. **12**, 456 (1991).
[7]W. P. Kang, J. L. Davidson, A. Wisitsora-at, D. V. Kerns, and S. Kerns, J. Vac. Sci. Technol. B **19**, 936 (2001).
[8]A. T. Sowers, B. L. Ward, S. L. English, and R. J. Nemanich, J. Appl. Phys. **86**, 3973 (1999).
[9]P. T. Joseph, N. H. Tai, H. Niu, U. A. Palnitkar, W. F. Pong, H. F. Cheng, and I. N. Lin, Diamond Relat. Mater. **17**, 1812 (2008).
[10]Y. C. Lee, S. J. Lin, I. N. Lin, and H. F. Cheng, J. Appl. Phys. **97**, 054310 (2005).
[11]C. F. Shih, K. S. Liu, and I. N. Lin, Diamond Relat. Mater. **9**, 1591 (2000).
[12]V. I. Polyakov, N. M. Rossukanyi, A. I. Rukovishnikov, S. M. Pimenov, A. V. Karabutov, and V. I. Konov, J. Appl. Phys. **84**, 2882 (1998).
[13]Y. H. Chen, C. T. Hu, and I. N. Lin, Appl. Phys. Lett. **75**, 2857 (1999).
[14]A. Lamouri, Y. Wang, G. T. Mearini, I. L. Krainsky, J. A. Dayton, Jr., and W. Mueller, J. Vac. Sci. Technol. B **14**, 2046 (1996).
[15]P. C. Huang, W. C. Shih, H. C. Chen, and I. N. Lin, Jpn. J. Appl. Phys., Part 1 **50**, 08KE04 (2011).
[16]P. C. Huang, W. C. Shih, H. C. Chen, and I. N. Lin, J. Appl. Phys. **109**, 084309 (2011).
[17]T. D. Corrigan, D. M. Gruen, A. R. Krauss, P. Zapoa, and R. P. H. Chang, Diamond Relat. Mater. **11**(1), 43–48 (2002).
[18]Y. C. Lee, S. J. Lin, I. N. Lin, and H. F. Cheng, J. Appl. Phys. **7**(5), 054310 (2005).
[19]R. H. Fowler and L. Nordheim, Proc. R. Soc. London, Ser. A **119**, 173 (1928).
[20]Z. Sun, J. R. Shi, B. K. Tay, and S. P. Lau, Diamond Relat. Mater. **9**, 1979 (2000).
[21]A. C. Ferrari and J. Robertson, Phys. Rev. B **63**, 121405 (2001).
[22]J. Michler, Y. Von Kaenel, J. Stiegler, and E. Blank, J. Appl. Phys. **81**(1), 187 (1998).
[23]A. C. Ferrari and J. Robertson, Phys. Rev. B **61**, 14095 (2000).
[24]I. N. Lin, H. C. Chen, C. S. Wang, Y. R. Lee, and C. Y. Lee, Cryst. Eng. Comm. **13**, 6082 (2011).
[25]W. C. Chiou, Jr. and E. A. Carter, Surf. Sci. **530**, 87 (2003).
[26]S. Jiao, A. Sumant, M. A. Kirk, D. M. Gruen, A. R. Krauss, and O. Auciello, J. Appl. Phys. **90**(1), 118 (2001).
[27]P. Zapol, M. Sternberg, L. A. Curtiss, T. Frauenheim, and D. M. Gruen, Phys. Rev. B **65**, 045403 (2001).